Cement and Concrete Research 40 (2010) 723–730

Contents lists available at ScienceDirect

Cement and Concrete Research

journal homepage: http://ees.elsevier.com/CEMCON/default.asp

Interaction between two anti-graffiti treatments and cement mortar (paste)

P.M. Carmona-Quiroga [a,*], S. Martínez-Ramírez [a], I. Sobrados [b], M.T. Blanco-Varela [a]

[a] Instituto de Ciencias de la Construcción Eduardo Torroja (CSIC), C/ Serrano Galvache 4, 28033 Madrid, Spain
[b] Instituto de Ciencia de Materiales (CSIC), C/ Sor Juana Inés de la Cruz, 3, 28049 Cantoblanco-Madrid, Spain

ARTICLE INFO

Article history:
Received 27 August 2009
Accepted 6 January 2010

Keywords:
Cement paste (D)
Mortar (E)
Thermal analysis (B)
^{29}Si MAS NMR
Anti-graffiti coatings

ABSTRACT

Much of the twentieth century's built heritage is made of concrete, which is particularly susceptible to graffiti "attacks". Since the traditional methods used to remove spray paint are not particularly effective on this type of material, the adoption of preventive measures by applying a new type of protective treatments, known as anti-graffiti coatings, may be a good way to tackle the problem. The present study aimed to evaluate the physical properties of a cement mortar coated with two such products and to study the possible molecular interactions between the coatings and the cement paste. Neither product induced chromatic changes on the surface of the material, while both made it water repellent. ^{29}Si MAS NMR analysis detected a lower Q^1/Q^2 ratio, indicative of a longer chain length, in the C–S–H gel in the cement paste mixed with the anti-graffiti products.

1. Introduction

Much of the twentieth century's concrete built heritage is exposed to graffiti, a form of vandalism that carries a heavy social and economic impact (degradation and devaluation of the areas affected and high cleaning costs) [1].

Graffiti must be removed as quickly as possible to deter future attacks and prevent the paint from interacting or combining chemically with air pollution, which renders cleaning more difficult [2].

The removal methods presently in place, based on either the use of specific products (chemical cleaning) or machinery, i.e. air or water guns, planers, brushes, cutters and similar (physical–mechanical cleaning) [3,4], do not always achieve satisfactory results. While graffiti can be removed from plastic, metal or ceramic tile with relative ease, it is very difficult to eliminate completely from concrete or natural stone [5].

Since spray paint removal necessarily involves an alteration in surface characteristics, the conviction that prevention is an effective option is gaining ground. A new type of specific surface treatments, anti-graffiti coatings, is available on the market. These products constitute a protective barrier against vandalism and facilitate graffiti removal by generating low energy surfaces that make the substrate water- and oil-repellent [6,7]. As a rule, graffiti applied to these protective barriers can be removed with low pressure water and a detergent or solvents [4].

Like any other protective treatment, they must be water- (and oil-) repellent, permeable to water vapour and chemically and photochemically stable, and bond well to the substrate without altering its colour or gloss [8,9].

For years, wax or micro-wax coatings (treatments that are removed with the paint) and polyurethane substances (permanent treatments) have held graffiti painters at bay. Such conventional anti-graffiti products have not solved the problem altogether, however, due to certain drawbacks to their use and their limited durability. Indeed, the former deteriorate in a matter of a few years when exposed to UV radiation, accumulate urban pollution that darkens the surface and may induce substantial decreases in permeability [10]. Polyurethanes, in turn, substantially change the appearance of the surfaces treated and create a vapour-proof seal that accelerates decay as a result of damp, salt crystallization and condensation underneath the treated surfaces [11].

The continuous launch of new anti-graffiti formulas or reformulations of existing coatings stands as proof of both the widespread use of measures to prevent graphic vandalism and the dissatisfaction with the results of the products available [12]. Indeed, surface treatments are often applied without a full understanding of substrate properties or choice of the optimal molecular structure for the type of prevention pursued, leading to insufficient protection or even decay of the materials involved.

Two permanent anti-graffiti coatings were selected for the present study: a fluorinated commercial one (a water-based fluoroalkylsiloxane) and an *o*rganically *mo*dified *sili*cate (Ormosil) synthesized from a polymer chain (polydimethyl siloxane, PDMS) and two network-forming alkoxides (Zr propoxide and methyltriethoxy silane, MTES) dissolved in n-propanol [13].

The present study aimed to ascertain the colour modification, hydric properties, porosity and vapour permeability of cement mortars treated with the two anti-graffiti coatings, and explore

* Corresponding author. Tel.: +34 913020440; fax: +34 913026047.
E-mail address: paulacq@ietcc.csic.es (P.M. Carmona-Quiroga).

0008-8846/$ – see front matter © 2010 Elsevier Ltd. All rights reserved.
doi:10.1016/j.cemconres.2010.01.002

possible chemical interactions between such products and hydrated cement paste, about which little is known at this time.

2. Experimental

2.1. Materials

Mortar specimens measuring 7×6×1 cm were prepared with CEM I 42.5 N cement, a sand/cement ratio of 3/1 and a water/cement ratio of 1/2 and cured for 28 days at 21 °C and 95% relative humidity as specified in Spanish and European standard UNE-EN 196-1 [14].

These specimens were coated with two permanent anti-graffiti treatments: a fluorinated commercial treatment [15] and a modified organic silicate (Ormosil) [13]. The products were deposited on to the substrates (one coat) by brushing.

The slices used for the contact angle trials (measuring approximately 2.5×2×0.3 cm), however, were immersed in the products for 1 min to ensure that they were fully coated. The amount of product deposited on the surface with the two methods is given in Table 1. The treated samples were allowed to dry at an ambient temperature to a constant weight (48 h, when the difference between two successive weightings, at a time interval of 24 h, is not more than 0.1% of the mass of the sample). More active residue remained on the immersion-coated and Ormosil samples.

The interaction between the anti-graffiti products and the hydrated cement paste was studied on cement paste specimens of the size and under the curing conditions described above, which were subsequently crushed and sieved to separate the fraction measuring from 250 to 425 μm. That fraction was coated with the two anti-graffiti treatments by immersing and stirring 1 g in 25 cm^3 of the diluted commercial product (5 and 75% vol. in water) and 1 g in 10 cm^3 of diluted Ormosil (also 5 and 75% vol.). The samples were subsequently filtered and dried for 16 h in a kiln at 40 °C and re-sieved through 250- and 425-μm sieves.

The anti-graffiti treatments alone were reticulated at an ambient temperature, the commercial one for only 24 h due to the evaporation of the solvent (water) and Ormosil, synthesized under a sol–gel method, for one week to complete the gelification.

2.2. Techniques

A handheld Minolta CM 2500 D spectrophotometer was used to measure the chromatic coordinates of the coated and uncoated surfaces of the mortar specimens. Measurements were taken on dry samples in a laboratory environment under the following conditions: $L^*a^*b^*$ colour space, illuminant D65 (daylight with ultraviolet radiation) and a 10° viewing angle. The chromatic changes in the samples after coating with the protective treatments were also expressed in terms of total colour variation $\Delta E^*(\Delta E^* = (\Delta L^{*2} + \Delta a^{*2} + \Delta b^{*2})^{1/2})$ [16]. Surface gloss was determined with a handheld Minolta Multi Gloss 268 gloss meter at a specular reflection angle of 85°.

Porosity and pore size distribution of the cement mortar before and after coating were studied on irregularly shaped fragments of the mortar specimens with a Micromeritics Autopore IV 9500 V1.05 mercury porosimeter. The water repellence afforded by the treatments was evaluated with dynamic contact angle measurements obtained with a CAHN DCA-315 microbalance.

Table 1
Anti-graffiti coating residues.

	Residue (% mass)			
	Brush (1 coat)		Immersion (1 min)	
	Commercial	Ormosil	Commercial	Ormosil
Cement mortar	0.33 ± 0.03	0.48 ± 0.08	1.24 ± 0.15	1.97 ± 0.62

The porosity accessible to water and low water pressure absorption values of the cement mortar coated and uncoated was found as recommended by RILEM [17,18]. The saturation coefficient was determined from the following expression $S = (W_2 - W_1)/W_1 * 100$, where W_1 represents the sample dry weight and W_2 the weight after saturation for 48 h at an atmospheric pressure. Water vapour permeability was found by determining gravimetric variation with the wet cup method (in which the sample is sealed to the top of a cup containing a saturated saline solution and placed in a kiln at 40 °C in which the relative humidity is also controlled) [9].

The dried treatments and the coated and uncoated pastes were characterized with FTIR, ^{29}Si MAS NMR and TG-DSC.

KBr pellets were prepared for the infrared spectra (300 mg of KBr and 1 mg of sample). Sixty four scans were read on an ATI Mattson Genesis spectrometer across an interval of 4000–400 cm^{-1} at a spectral resolution of 4 cm^{-1}.

The ^{29}Si MAS NMR spectra were recorded at 79.49 MHz on a Bruker AVANCE-400 spectrometer using an external magnetic field of 9.4 T. Measurements were taken at 20 °C and the samples were spun around the magic angle (54°44′ with respect to the magnetic field) at a rate of 10–12 kHz. The pulse length was π/2 per 5 μs, with 5-second intervals between accumulated scans. The ^{29}Si chemical shifts were referred to $(CH_3)_4Si$. The MAS NMR single pulse spectra were deconvoluted with Origin 6.0 software to determine the components and their contributions, assuming a normal distribution.

A TA SDT Q600 thermal analyzer was used to conduct thermogravimetric and heat flow analyses on the coated and uncoated cement pastes and air-dried anti-graffiti coatings, using the platinum and aluminium crucibles as references. The samples were heated to 1050 °C in an air atmosphere at a rate of 4 °C/min.

3. Results and discussion

3.1. Physical characterization of the coated mortar

Neither of the treatments changed specimen surface colour or gloss (Table 2). The changes in parameters L^* and b^* observed after the mortar was coated can be related to the characteristics of the material itself and its preparation. In fact the variations in total colour (ΔE^*) found, which were under 5 units, were not visible to the naked eye [19].

The physical and hydric properties of the mortar are given in Table 3. Mercury intrusion porosimetry revealed that the treatments obstructed mortar pores in different ways. Total mortar porosity, at 9.3%, primarily comprising pores with a diameter of under 0.1 μm in the cementitious matrix, remained unchanged after applying the commercial product. On the contrary, Ormosil reduced this value by 38%, filling pores smaller than 0.1 μm (pores with a diameter of under 0.01 μm disappeared altogether).

Saturation (48 h at an atmospheric pressure) values were similar for the substrate coated with the marketed anti-graffiti and the uncoated substrate: 5.1% (mass) and 5.6%, respectively. This finding is

Table 2
Chromatic parameters on the cement mortar surface untreated and treated with the anti-graffiti coatings. L^*, lightness; a^*, red/green hue; b^*, yellow/blue hue; C, chroma ($C^* = (a^{*2} + b^{*2})^{1/2}$); ΔE^*, total colour variation ($\Delta E^* = (\Delta L^{*2} + \Delta a^{*2} + \Delta b^{*2})^{1/2}$); GU, gloss units.

	Uncoated	Commercial	Ormosil
L^*	75.8 ± 2.7	73.5 ± 1.4	74.7 ± 4
a^*	0.2 ± 0	0.1 ± 0.1	0.2 ± 0
b^*	4.2 ± 1	5.3 ± 0.5	4.3 ± 1
C^*	4.2 ± 1	5.3 ± 0.5	4.3 ± 1
ΔE^*	–	2.6 ± 1.5	3.4 ± 1
GU	1.6 ± 0.4	1.6 ± 0.3	2 ± 0.4

Table 3
Physical and hydric properties of cement mortar untreated and treated with the anti-graffiti coatings.

	Uncoated	Commercial	Ormosil
Porosity accessible to Hg (%)	9.3 ± 1.2	9.4 ± 0.8	5.7 ± 1.2
>0.1 μm (paste–aggregate interface)	3.2 ± 1.7	4 ± 0.6	4 ± 1
<0.1 μm (matrix)	6.1 ± 3	5.5 ± 0.2	1.8 ± 0.1
Porosity accessible to water (% volume)	9.2 ± 0.1	8.1 ± 0.2	5.5 ± 0.2
Saturation coefficient (% mass)	5.6 ± 0	5.1 ± 0	3 ± 0.1
60-minute low water pressure absorption (kg/m^2 h)	2.6	1.7	0.1
Advancing angle (°)	48.4 ± 5	117.4 ± 6.4	120.2 ± 6.6
Receding angle (°)	–	61.3 ± 0.7	45 ± 6.2
Decrease in water vapour permeability[a] (%)	–	10.2 ± 6.2	30.4 ± 2.1

[a] $0.89*10^{-11}$ kg/m s Pa.

consistent with the minimal decrease in porosity accessible to water induced by this treatment (Table 3). By contrast, in the Ormosil-coated samples, the amount of water freely absorbed by the material decreased significantly.

The low pressure water absorption test results (Table 3) showed that the cement mortar absorbed water at a rate of 2.6 kg/m^2 h. This value decreased to 1.7 kg/m^2 h in the commercial product-coated mortar and even more steeply in the Ormosil specimens, for which the value was characteristic of well protected porous surfaces (<0.35 kg/m^2 h) [20].

Cement mortars are porous, somewhat water vapour-permeable materials. Surface treatments may reduce such permeability, substantially shortening durability [21,22].

The water vapour permeability in the cement mortar studied, $0.89*10^{-11}$ kg/m s Pa (much higher than reported by Frattolillo et al. [23] in a mortar with a slightly lower w/c ratio ($0.12*10^{-11}$ kg/m s Pa)) decreased by only 10.2% with the commercial anti-graffiti, while Ormosil lowered permeability by 30.4% (Table 3). Puterman [24] found sharper decreases than observed for the marketed product: permeability fell in a cement, lime and sand mortar by 20.9% when coated with a methyl siliconate, 31.3% when the protective coating was a urethane-modified silicone, and 26.8 and 32.5% when siloxanes were used.

The contact angle measurements (Table 3) showed that the cement mortar treated with the two coatings was more water repellent than the control sample. The advancing angle (θa) increased substantially and to similar values with the two anti-graffiti products. Water sorptivity values in the uncoated cement mortar were too high to obtain receding angle (θr) measurements. Since the specimens coated with the commercial treatment exhibited higher θr values than the Ormosil samples, the former may be considered a slightly more effective water repellent. The apparent contradiction between this observation and the findings showing the greater capacity of Ormosil to reduce the value of all cement hydric properties and porosity may be explained by the fact that the receding angle actually refers to an aspect other than surface characterization, as discussed below.

The use of the advancing or receding angle to determine the effectiveness of surface treatments may on occasion lead to incorrect interpretations [25,26].

As the studies on stone conducted by Brugnara et al. [26] showed, the advancing angle, θa, increases immediately after application of a surface coating even at small product concentrations (0.5% w/w), whereas θr only climbs when concentrations of over 6% w/w are used. Hence, an advancing angle on the order of 140° determined by these authors [26] for a very rough and porous calcarenite (30–35%), which should have indicated that the surface was extremely water repellent (water penetration in capillary pores is theoretically impossible at angles of over 90°), was related, on the contrary, to high water absorption.

According to Tsakalof et al. [27], the static contact angle is related to instantaneous (short-term) surface water repellence, whereas capillary water uptake represents long-term repellence.

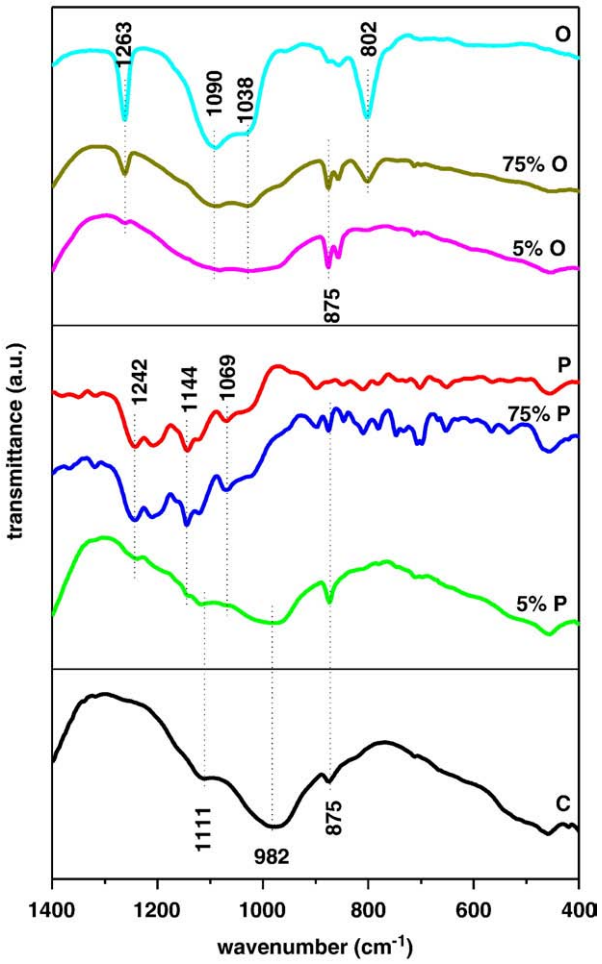

Fig. 1. Infrared spectra for cement paste (C), paste mixed with 5% of commercial anti-graffiti (5% P), paste mixed with 75% commercial anti-graffiti (75% P), commercial anti-graffiti (P), paste mixed with 5% Ormosil (5% O), paste mixed with 75% Ormosil (75% O) and Ormosil (O).

The advancing angle is related to the most hydrophobic portion of a surface while the receding angle is related to higher energy areas where water absorption takes place [26] and therefore the second one represents instantaneous water repellence more accurately.

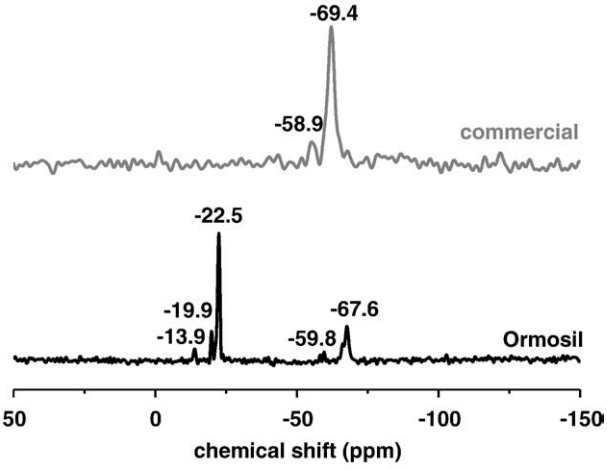

Fig. 2. ^{29}Si MAS NMR spectra for two dry anti-graffiti coatings, the commercial one and the Ormosil.

The amount of low water pressure water absorbed by the cement mortar (pipe test), would therefore represent long-term water repellence, where surface porosity plays an important role, as can be seen in close correlation between the two parameters.

Consequently, the commercial anti-graffiti is more water repellent than Ormosil in the short term, according to the receding dynamic contact angle findings, while in the longer term, according to the low water pressure absorption test, Ormosil would exhibit higher performance, due to its capacity to fill the pores in the material.

3.2. Chemical interaction between paste and anti-graffiti coatings

3.2.1. FTIR

In Fig. 1 the infrared spectra of the cement paste and of their mixtures with the diluted treatments (5 and 75% vol. in solvent) revealed that the two products were absorbed differently by the powdered material (250–425 μm).

When the paste was mixed with the most diluted form (5%) of the marketed product (Fig. 1, 5% P), the most clearly distinguishable bands were generated by silicate (982 cm^{-1}), sulfate (1111 cm^{-1}), carbonate (875 cm^{-1}) and portlandite (3642 cm^{-1}, band not shown) vibrations [28]. When the product concentration was increased (Fig. 1, 75% P), the substrate bands were barely visible, while the bands for the commercial treatment (the most prominent signals between 1242 and 1069 cm^{-1}), which was readily absorbed by the cement paste, could be distinctly seen.

The infrared spectra for the samples mixed with the two concentrations of Ormosil were similar (Fig. 1, 5% O and 75% O). While the intensity of the main vibration bands for the treatment increased at the higher concentration (at 1263 cm^{-1} (symmetric bending in CH_3), 1090 cm^{-1}, 1038 cm^{-1} (asymmetric stretching in

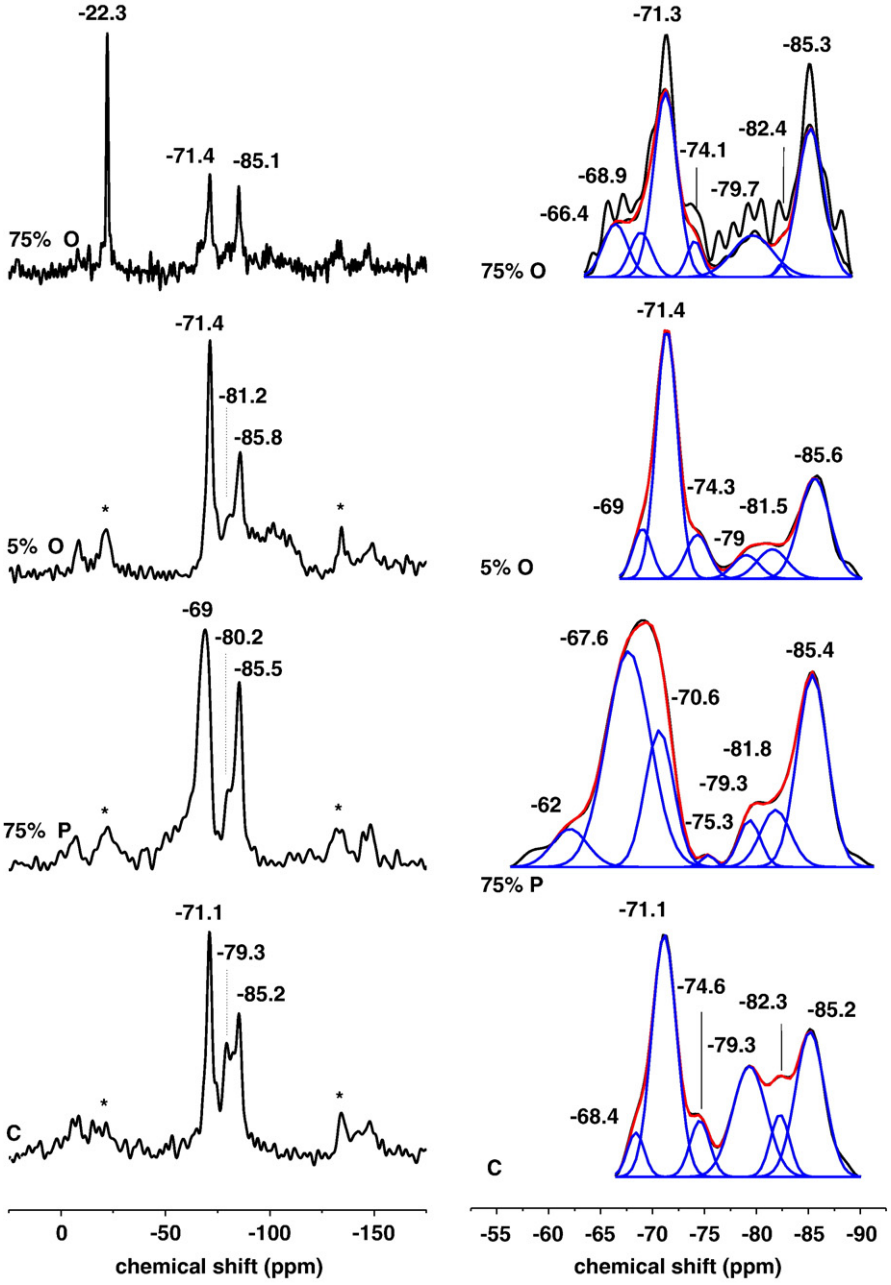

Fig. 3. ^{29}Si NMR spectra for cement paste (C), paste mixed with 75% commercial anti-graffiti (75% P), paste mixed with 5% Ormosil (5% O) and paste mixed with 75% Ormosil (75% O). On the right, the deconvoluted spectra.

Table 4
Area percentage of signals Q^1 and Q^2 for cement paste (C) and for their mixtures with two anti-graffiti coatings: 75% commercial treatment (75% P) and 5 and 75% Ormosil (5% O and 75% O).

	$Q^1/\Sigma Q^{1+2}$	$Q^2/\Sigma Q^{1+2}$
C	41	59
75% P	11	89
5% O	13	87
75% O	30	70

Si–O–Si, symmetric stretching in Si–O–C respectively) and 802 cm^{-1} (symmetric stretching in Si–O–Si and asymmetric stretching in Si–C) [29,30]), the substrate signals were visible in both.

Neither new bands that would denote substrate–treatment interactions (formation of covalent bonds) were detected on the infrared spectra for the coated samples, nor was any shift in the existing bands observed [31].

3.2.2. ^{29}Si MAS NMR

Magnetic resonance of ^{29}Si nuclei was used to analyze possible interactions between the paste and the anti-graffiti coatings, which may affect both the effectiveness of the protective treatments and substrate durability [32,33].

Fig. 2 shows the ^{29}Si MAS NMR spectra for the two anti-graffiti products, dried at room temperature. The most intense signal on the spectrum for the commercial product, at −69.4 ppm, was attributed to T^3 ($R'Si(OSi)_3$) three dimensional structures, while the resonance at −58.9 ppm was attributed to T^2 ($R'Si(OSi)_2OR$) structures [15]. In Ormosil the resonances were due to the Si atoms in T and D units. The most intense, at −22.5 ppm, was attributed to the D^2 ($R'_2Si(OSi)_2$) units in the long PDMS chains (main Si atoms in the PDMS skeleton bound to only two C atoms), as was the signal at −19.9 ppm (near the cross-linked points) [34]. The resonance at −13.9 ppm (D^1, $R'_2Si(OSi)OR$ [35]), in turn, was attributed to the terminal Si atoms bound to hydroxyl groups in the PDMS molecule [36]. The signals at −67.6 and −59.6 ppm were respectively assigned to T^3 ($R'Si(OSi)_3$) and T^2 ($R'Si(OSi)_2OR$) structures [37] in the totally and partially hydrolyzed MTES.

Fig. 3 shows the ^{29}Si MAS NMR spectrum for the cement paste (C), with three resonances, at −71.1, −79.3 and −85.2 ppm. The first was attributed to unreacted belite (Q^0) [38]. The second and third were respectively assigned to the Si in Q^1 and Q^2 positions, i.e., at the end and in the middle of the C–S–H gel chain. Spectrum deconvolution (Fig. 3, right, C), revealed three new resonances, at −68.4, −74.6 and −82.3 ppm. The former two were characteristic of the first two Q^0 units of monomeric silicon and the third to paired Q^2 Si units (Q^2(1Al)) [28,39] or bridge units with one OH (Q^2(1OH)) [40].

In the spectra for the cement–anti-graffiti product mixtures (Fig. 3), the commercial treatment peak at −69.4 ppm and the Ormosil peak at −67.6 ppm showed previously in Fig. 2 and attributed to T^3 ($R'Si(OSi)_3$) units, overlapped with the Q^0 signal generated by the anhydrous silicates of cement, clearly widening the signal, particularly when the coating was the commercial product diluted (75% P). Evidence of the interaction of the anti-graffiti products with the cement was found in the changes observed in the zone of the spectrum containing the resonances generated by the C–S–H gel chain units. The coatings induced a decrease in the percentage of Si atoms in Q^1 positions with respect to the Si in Q^2 positions (Fig. 3 and Table 4).

Although applying more concentrated Ormosil did not raise the Q^2/Q^1 ratio (Fig. 3 and Table 4), bearing in mind the low signal/noise ratio in the spectrum for the 75% Ormosil-coated paste (Fig. 3, 75% O), the signal area percentages calculated in this case (Table 4) may not be entirely representative.

This increase in the silicate chain length was also observed by Beaudoin et al. [41] when studying the interaction between organic compounds and C–S–H gel. The authors attributed this finding, which raised gel and consequently cement paste strength, to the inclusion of the organic molecules in the gel structure and/or their bonding to defect sites missing bridging tetrahedra.

3.2.3. TG-DSC

Cement paste thermogravimetric and DSC analysis was conducted in air before and after mixing with the two concentrations of the two anti-graffiti products. The products themselves were also analyzed.

Four mass loss stages (Table 5) were distinguished on the TG/DTG curves for dry commercial anti-graffiti (Fig. 4, P). The first, at approximately 100 °C, denoted water evaporation. A higher mass loss rate, whose origin was not identified, was recorded in the second (108–170 °C) at 146 °C. The most significant mass loss took place thereafter and up to 434 °C (79.77% of a total of 95.65%), as a result of the decomposition and oxidation of the majority carbo-fluorinated groups. After 434 °C the anti-graffiti product lost mass (8.17%) more slowly up to approximately 600 °C, at which temperature the material had decomposed completely.

The DSC curve for this sample (Fig. 4, P) exhibited two endothermal peaks at 51 and 98 °C, followed by exothermal peaks at 155, 217, 296, 359 and 457 °C. The endothermal peaks concurred with the first stage of mass loss, while the others corresponded to the mass losses in the second, third and fourth stages described in the preceding paragraph. Since mass losses took place simultaneously with exothermal reactions in the three last stages, they were interpreted to consist in oxidation/combustion reactions in the fluorinated and alkyl chains present in the polymer [42,43]. The temperature ranges at which decomposition was observed concurred with the values found in the literature. Monde et al. [42] reported a single exothermal signal at 435 °C in silica gels containing polyfluoroalkyl groups, whereas in a fluorinated polymer such as Teflon, fluorinated group oxidation and decomposition took place at a higher temperature, 540 °C [42].

Ormosil decomposition also proceeded in four stages (Fig. 4, TG, O, and Table 5). The gradual mass loss (4.3%) observed up to 269 °C was related to heat-induced residual silanol and terminal ethoxy group condensation [33]. From 269 to 435 °C (11.2% of a total of 52.8%) the loss was due to gel dehydroxylation. The third stage, where mass loss was steeper (35.4% from 435 to 526 °C), contained an exothermal signal peaking at 440 °C on the DSC curve. The width of this signal, attributed to the oxidation of the carbonated groups in the gel, was an indication of the wide range of oxidation temperatures and consequently of the diversity of environments around these units in

Table 5
Mass loss in cement paste (C), in their mixtures with 5 and 75% commercial anti-graffiti (5% P and 75% P), 5 and 75% Ormosil (5% O and 75% O) and in the commercial treatment (P) and Ormosil (O).

°C		C	5% P	75% P	P	5% O	75% O	O
25–100	H_2O	4.22	3.86	2.51	3.66	3.23	2.75	0.71
100–400	OH (gel, etc.)	6.83	8.37	47.89	71.07 (300–400 °C = 58.88%)	5.48	6.50	11.47
400–600	OH ($Ca(OH)_2$)	4.89	10.47	15.50	20.49	5.87	7.74	40.14
600–1050	CO_2	6.87	5	2.64	0.43	9.93	8.05	0.48
Total		22.81	27.7	68.54	95.65	24.51	25.04	52.8

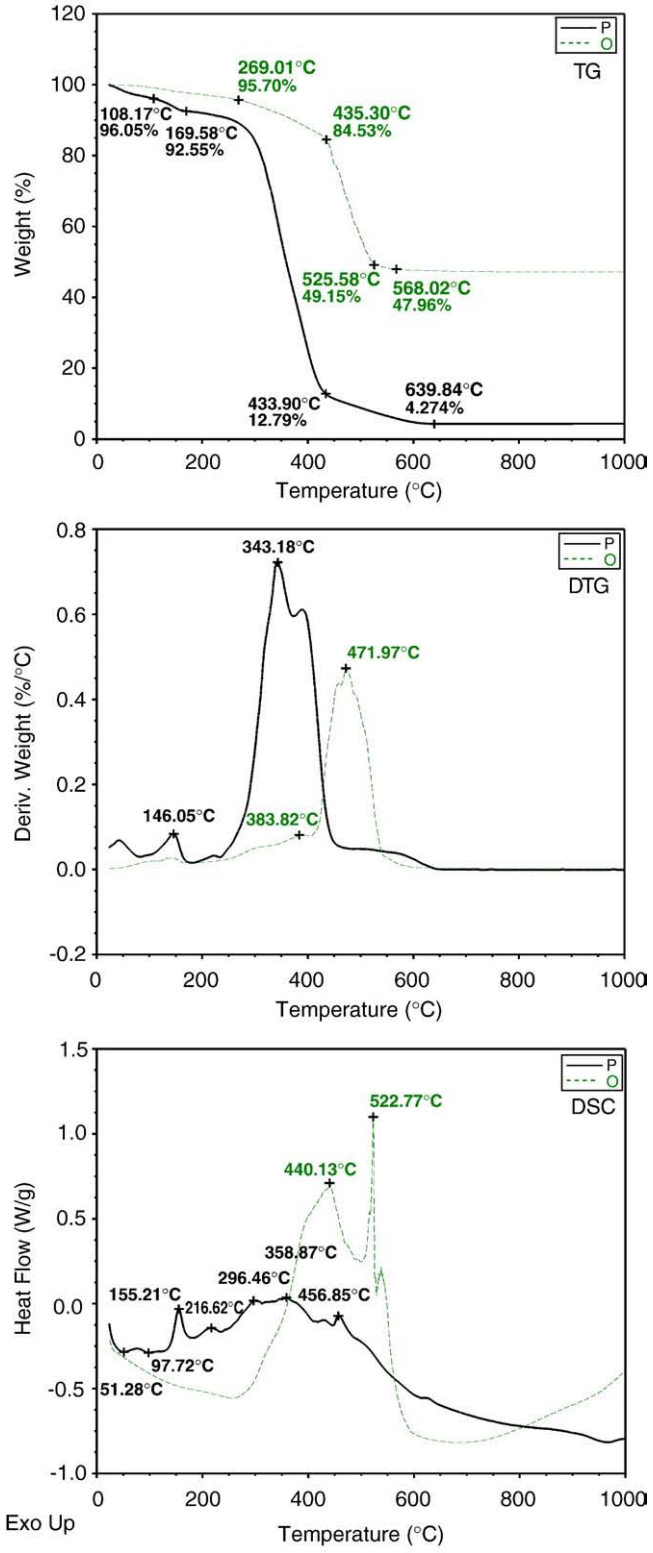

Fig. 4. From top, TG, DTG and DSC curves for commercial anti-graffiti (P) and Ormosil (O).

the gel [33]. Lastly, a small mass loss of only 1.2% was recorded between 526 and 568 °C. Another exothermal peak appearing in this range of temperatures, at 523 °C, might be attributed to the transformation of tetragonal to monoclinic ZrO_2. Aguilar et al. [44] detected this signal at somewhat lower temperatures, from 395 to 500 °C, in sol–gel ZrO_2–SiO_2 systems.

Heat flow analysis (Fig. 5, DSC, C) of the hydrated cement paste essentially revealed the presence of three types of endothermal signals related to water loss (at around 100 °C), the decomposition of portlandite (at 439 °C) and the release of the CO_2 in calcite (at around 700 °C). The presence of the most diluted form of the fluorinated anti-graffiti treatment (Fig. 5, DSC, 5% P) raised the portlandite dehydroxylation temperature slightly (by 6 °C) and lowered the decarbonation temperature by about 20 °C. In addition, an exothermal signal appeared at around 400 °C, generated by the combustion of the fluorocarbonated units in the polymer. The higher dehydroxylation temperature for $Ca(OH)_2$ may have been apparent only, i.e., the result of the overlap in exothermal commercial product combustion and endothermal portlandite dehydroxylation, which would shift the peak but not the end of the process, reducing the area of the peak observed. The lower decarbonation temperature, by contrast, may be related to the existence of a chemical interaction between the calcite particles and the polymer.

Only the exothermal signals for the marketed treatment were detected on the sample coated with the higher concentration of this product (Fig. 5, DSC, 75% P) at 309, 430 and 532 °C, which were due essentially to the decomposition and oxidation of its fluorinated groups (the third recorded at a higher temperature than on the heat flow curve for the polymer alone, Fig. 4, DSC, P, 457 °C). This was an indication of the large amount of treatment product readily absorbed by cement paste particles.

No significant differences were noted on the heat flow curve (Fig. 5, DSC, 5% O and 75% O) when the material was mixed with Ormosil, except that the more diluted solution (5% vol.) lowered the portlandite dehydroxylation temperature by 6 °C and raised the decarbonation temperature by 11 °C, while the more concentrated form (75% vol.) raised the portlandite decomposition temperature by 4 °C.

The DTG curve for the cement paste was characterized by the presence of peaks at 87, 433, 672 and 696 °C (Fig. 5, DTG, C). The paste mixed with the lower concentration of the commercial product had further two peaks, at 391 and 533 °C (Fig. 5, DTG, 5% P), characteristic of the decomposition of the fluorinated treatment (Fig. 4, DTG, P), which were the only visible signals (besides the water loss) on the DTG curve for the sample mixed with 75% commercial product (Fig. 5, DTG, 75% P).

Treating the cement paste particles with Ormosil appeared to retard the water loss from the C–S–H gel (Fig. 5, TG, 5% O and 75% O). Nonetheless, the percentage of mass loss due to portlandite dehydroxylation between approximately 416 and 445 °C (in the untreated cement paste) did not increase in the coated samples (2.5–2.6% in the coated materials and 2.8% in the control sample), indicating that gel water loss was not pushed back to this interval. Both concentrations of this treatment induced an increase in the rate of mass loss in the sample at around 600 °C (Fig. 5, TG, 5% O and 75% O), the result of the decomposition of its alkyl units, which was more intense at the higher concentration.

As the mass loss percentages in the samples at the temperature intervals selected show (Table 5), the presence of the coatings raised the total mass loss but lowered the initial loss (up to 100 °C), for the less water content in the larger pores (responsible of mass loss at temperature lower than 100 °C) when they are occupied by the treatments.

The marketed treatment caused an increase in the mass loss between 100 and 600 °C (Table 5, 5% P and 75% P), the temperature range in which the treatment lost 91.6% of its mass, of a total of 95.7%. The loss of CO_2 was lower from 600 to 1050 °C, particularly in the commercial product-coated sample (Table 5, 5% P and 75% P).

Total mass loss increased similarly in the Ormosil-coated specimens at the two concentrations used (1.7 and 2.2% for 5% and 75% Ormosil coating, respectively) (Table 5, 5% O and 75% O). The coated samples exhibited greater losses from 400 to 600 °C due to treatment decomposition. From 100 to 400 °C, however, the mass loss decreased despite treatment decomposition in this temperature range (mass loss of 11.47%). This may denote that the presence of the coating hindered water loss in the C–S–H gel or modified its OH content. Unlike the

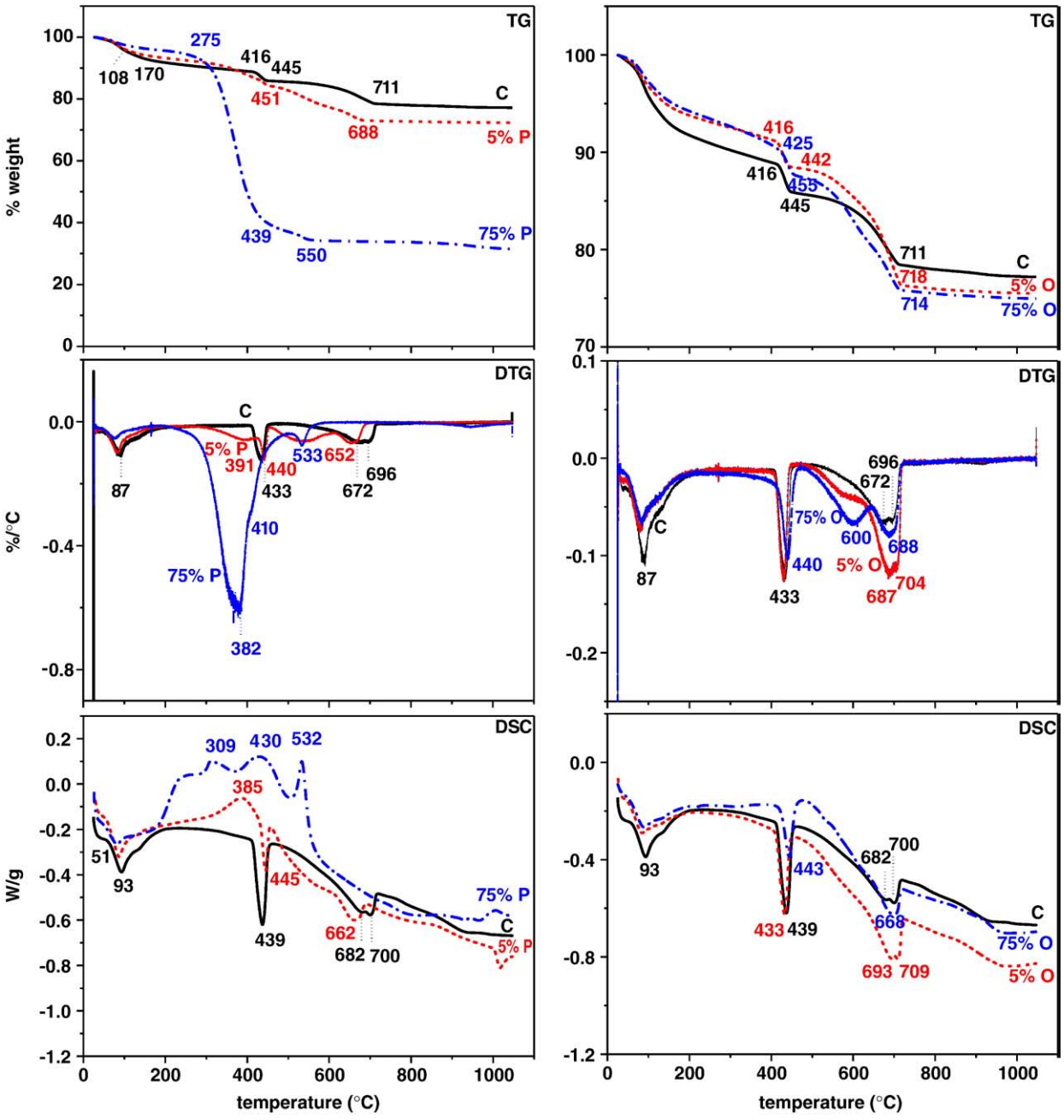

Fig. 5. From top, TG, DTG and DSC curves for cement paste (C) and paste mixed with 5% and 75% treatments: 5(75)% P (left) and 5(75)% O (right).

samples coated with the commercial anti-graffiti, in the pastes treated with Ormosil, the CO_2 loss grew despite the insignificant contribution of the treatment (0.48%), possibly indicating a higher degree of carbonation. The inflection at 600 °C on the DTG curves for the cement paste coated with Ormosil (Fig. 5, 5% O and 75% O) may denote the presence of a substrate–treatment interaction (Table 5).

4. Conclusions

1. Neither of the anti-graffiti treatments induced chromatic variations on the cement mortar surface.
2. While total mortar porosity (accessible to mercury and water) was not significantly modified by the commercial anti-graffiti, it was reduced by approximately 40% by Ormosil, which filled the pores, essentially the ones with a diameter of under 0.1 μm.
3. Ormosil reduced water vapour permeability by 30.4%, whereas the decrease with the marketed product was only 10.2%.
4. The Ormosil-coated mortar acquired long-term water repellence and exhibited a very low specific water absorption rate, lower than in the material coated with the commercial treatment.
5. The receding angle findings indicated that the commercial product afforded greater short-term water repellence.
6. ^{29}Si MAS NMR, revealed that the two anti-graffiti products reacted with C–S–H gel, raising the relative proportion of Si in Q^2 positions with respect to the Q^1 end-of-chain positions. This translates into a longer mean chain length. Infrared spectroscopy, on the contrary, proved to be poorly suited to studying the paste/coating chemical reaction.
7. Thermogravimetric and heat flow analysis confirmed the above interaction, given the decrease in dehydroxylation-related losses in the C–S–H gel between 100 and 400 °C induced by Ormosil, the lower decarbonation temperature induced by the marketed

treatment and the presence of an inflection at 600 °C in the DTG for Ormosil-coated samples.

Acknowledgements

One of the authors, Paula María Carmona Quiroga, benefited from an integrated employability pathway grant from the European Social Fund and the Spanish National Research Council, to whose Thematic Network on Cultural Heritage she is assigned. Dr. Juan Rubio of ICV (CSIC) and Ana de Pedro of Degussa are thankfully acknowledged for providing the anti-graffiti. This research was funded by the Spanish Ministry of Education and Science (Projects MAT 2003-08343 and CONSOLIDER CSD2007-00058).

References

[1] H. Dubin, Options and strategies for tackling graffiti, Construct. Specif. 55 (8) (2002) 53–54.
[2] http://www.english-heritage.org.uk/server/show/nav.1049 (Graffiti Removal, English Heritage).
[3] F. Piacenti, Chemistry for the conservation of the cultural heritage, Sci. Total Environ. 43 (1) (1994) 113–120.
[4] M.E. Weaver, Removing graffiti from historic masonry. Preservation briefs 38. Technical preservation services. National Park Service. U.S. Department of Interior. http://www.nps.gov/hps/tps/briefs/brief38.htm.
[5] P. Sanjeevan, A.J. Klemm, P. Klemm, Removal of graffiti from the mortar by using Q-switched Nd:YAG laser, Appl. Surf. Sci. 253 (20) (2007) 8543–8553.
[6] A.J. Hutchinson, L.J. Hyde, V.G. Gomes, Engineering an anti-graffiti system: a study in industrial product design, Chem. Eng. Technol. 27 (8) (2004) 874–879.
[7] Z. Dobkowski, M. Zielecka, The physicochemical characterization of fluropolymer-modified polysiloxane coatings, Polimery 46 (11–12) (2001) 835–839.
[8] M. Levi, C. Ferro, D. Regazzoli, G. Dotelli, A. Lo Presti, Comparative evaluation method of polymer surface treatments applied on high performance concrete, J. Mater. Sci. 37 (22) (2002) 4881–4888.
[9] M. Álvarez de Buergo Ballester, R. Fort González, Basic methodology for the assessment and selection of water-repellent treatments applied on carbonatic materials, Prog. Org. Coat. 43 (4) (2001) 258–266.
[10] I. Maxová, R. Slesinger, O. Kubová, Test of some antigraffiti systems for preservation of sandstone monuments, 7th European Conference "SAUVEUR". Safeguarded Cultural Heritage. Understanding & Viability for the Enlarged Europe, vol. 2 (posters), Prague, May 31–June 3 2006, 831–833. Ed. M. Drdácký, M. Chapuis. http://www.arcchip.cz/ec-conference/download/B-827_897.pdf.
[11] Stone cleaning, paint removal and graffiti treatment, The city of Edinburgh Council, http://download.edinburgh.gov.uk/DQ_Guidelines/Stonecleaning_etc.pdf.
[12] A. Tarnowski, X. Zhang, C. McNamara, S.T. Martin, R. Mitchell, Biodeterioration and performance of anti-graffiti coatings on sandstone and marble, J. Can. Assoc. Conserv. 32 (2007) 3–16.
[13] J.L. Oteo, J. Rubio, F. Rubio, F. (CSIC), Spanish patent no. 9901977.
[14] UNE-EN 196-1: 2005, Methods of testing cement—part 1: determination of strength.
[15] P.M. Carmona-Quiroga, S. Martínez-Ramírez, M.T. Blanco-Varela, Fluorinated anti-graffiti coating for natural stone, Mater. Constr. 58 (289–290) (2008) 233–246.
[16] Commission Internationale de l'Eclairage (CIE), Colorimetry, Bureau central de la CIE, Paris, , 1986.
[17] Commission 25-PEM Protection et Érosion des Monuments, test no. I. 1. Porosity accessible to water, Matériaux de Constructions 13 (75), RILEM, Paris, 1980, pp. 177–179.
[18] Commission 25-PEM Protection et Érosion des Monuments, water absorption under low pressure (pipe method), Matériaux de Constructions 13 (75), RILEM, Paris, 1980, pp. 201–205.
[19] F. Di Gennaro, A. Ferrari, C. Pagella, G. Cervellati, Petrographic study on efectiveness of antigraffiti protective treatment (part 1—stony materials of carbonatic composition), Pitture e Vernici, Eur. Coat. 78 (17) (2002) 23–31.
[20] S.O. Nwaubani, J. Dumbelton, A practical approach to in-situ evaluation of surface-treated structures, Constr. Build. Mater. 15 (4) (2001) 199–212.
[21] C.D. Vacchiano, L. Incarnato, P. Scarfato, D. Acierno, Conservation of tuff-stone with polymeric resins, Constr. Build. Mater. 22 (5) (2008) 855–865.
[22] H. Ling, N. Maiqian, L. Guozheng, Preparation and feasibility analysis of fluoropolymer to the sandstone protection, Prog. Org. Coat. 62 (2) (2008) 206–213.
[23] A. Frattolillo, G. Giovinco, M.C. Mascolo, A. Vitale, Effects of hydrophobic treatment on thermophysical properties of lightweight mortars, Exp. Therm. Fluid Sci. 30 (1) (2005) 27–35.
[24] M. Puterman, Hydrophobic materials—how effective are they? in: V. Fassina (Ed.), Proceedings of 9th International Congress on Deterioration and Conservation of Stone, Venice, 19–24 June, Elsevier Science, Amsterdam, 2000, pp. 443–452.
[25] P. Cardiano, S. Sergi, M. Lazzari, P. Piraino, Epoxy–silica polymers as restoration materials, Polymer 43 (25) (2002) 6635–6640.
[26] M. Brugnara, C. Della Volpe, A. Penati, S. Siboni, T. Poli, L. Toniolo, Correct use of the contact angle in the evaluation of the protective action induced from polymer coating on the stone, Ann. Chim-Rome 93 (2003) 881–888.
[27] A. Tsakalof, P. Manoudis, I. Karapanagiotis, I. Chryssoulakis, C. Panayiotou, Assessment of synthetic polymeric coatings for the protection and preservation of stone monuments, J. Cult. Herit. 8 (1) (2007) 69–72.
[28] R.A. Hanna, P.J. Barrie, C.R. Cheeseman, C.D. Hills, P.M. Buchler, R. Perry, Solid state ^{29}Si and ^{27}Al NMR and FTIR study of cement pastes containing industrial wastes and organics, Cem. Concr. Res. 25 (7) (1995) 1435–1444.
[29] L. Téllez, F. Rubio, R. Peña-Alonso, J. Rubio, Seguimiento por espectroscopía infrarroja (FT-IR) de la copolimerización de TEOS (tetraetilortosilicato) y PDMS (polidimetilsiloxano) en presencia de tbt (tetrabutiltitanio), Bol. Soc. Esp. Ceram. Vidr. 43 (2004) 883–889.
[30] R. Peña Alonso, F. Rubio, J. Rubio, J.L. Oteo, Characterisation of the pyrolysis process of boron-containing Ormosils by FT-IR analysis, J. Anal. Appl. Pyrol. 71 (2) (2004) 827–845.
[31] A. D'Alessio, F. Turchi, P. Narducci, P. Vergamini, F. Ciardelli, S. Catanorchi, Fluorinated polymers as stone-protective materials: an FTIR study on intermolecular interactions, Polym. Int. 53 (10) (2004) 1567–1571.
[32] E. Zendri, G. Biscontin, I. Nardini, S. Riato, Characterization and reactivity of silicatic consolidants, Constr. Build. Mater. 21 (5) (2007) 1098–1106.
[33] J. Brus, M. Skrdlantova, ^{1}H MAS NMR study of structure of hybrid siloxane-based networks and the interaction with quartz filler, J. Non-Cryst. Solids 281 (1–3) (2001) 61–71.
[34] R. Peña-Alonso, F. Rubio, J. Rubio, J.L. Oteo, The role of γ-aminopropyltriethoxysilane (γ-APS) on the thermal stability of TEOS-PDMS Ormosils, J. Sol–Gel Sci. Technol. 36 (1) (2005) 77–85.
[35] S.K. Young, W.L. Jarrett, K.A. Mauritz, Nafion®/ORMOSIL nanocomposites via polymer-in situ sol–gel reactions. 1. Probe of ORMOSIL phase nanostructures by ^{29}Si solid-state NMR spectroscopy, Polymer 43 (8) (2002) 2311–2320.
[36] J.D. Mackenzie, Y.J. Chung, Y. Hu, Rubbery ormosils and their applications, J. Non-Cryst. Solids 147–148 (1992) 271–279.
[37] B. Améduri, B. Boutevin, J.J.E. Moreau, H. Moutaabbid, M.W.C. Man, Hybrid organic–inorganic gels containing perfluoro-alkyl moieties, J. Fluorine Chem. 104 (2) (2000) 185–194.
[38] J. Skibsted, J. Hjorth, H.J. Jakobsen, Correlation between ^{29}Si NMR chemical shifts and mean Si–O bond lengths for calcium silicates, Chem. Phys. Lett. 172 (3–4) (1990) 279–283.
[39] I.G. Richardson, The nature of C–S–H in hardened cements, Cem. Concr. Res. 29 (8) (1999) 1131–1147.
[40] F. Brunet, Ph. Bertani, Th. Charpentier, A. Nonat, J. Virlet, Application of ^{29}Si homonuclear and ^{1}H–^{29}Si heteronuclear NMR correlation to structural studies of calcium silicate hydrates, J. Phys. Chem. B 108 (40) (2004) 15494–15502.
[41] J.J. Beaudoin, L. Raki, R. Alizadeh, A ^{29}Si MAS NMR study of modified C–S–H nanostructures, Cem. Concr. Comp. 31 (8) (2009) 585–590.
[42] T. Monde, H. Fukube, Y. Nemoto, T. Yoko, T. Konakahara, Preparation and surface properties of silica-gel coating films containing branched-polyfluoroalkylsilane, J. Non-Cryst. Solids 246 (1–2) (1999) 54–64.
[43] J.-S. Lee, Thermal decomposition of fluoropolymers and firing characteristics of priming compositions with fluoropolymers, J. Appl. Polym. Sci. 97 (5) (2005) 2054–2059.
[44] D.H. Aguilar, L.C. Torres-Gonzalez, L.M. Torres-Martinez, T. Lopez, P.A. Quintana, Study of the crystallization of ZrO_2 in the sol–gel system: ZrO_2–SiO_2, J. Solid State Chem. 158 (2) (2001) 349–357.